

# JGR Atmospheres

## RESEARCH ARTICLE

10.1029/2023JD040030

### Key Points:

- We developed a physically based phase classification scheme for two typical types of soundings by incorporating the atmospheric energy
- We greatly improved phase prediction for Type 2 sounding, which features a melt-and-refreeze process poorly represented by prior methods
- We evaluated the phase classification with a 50% snow probability threshold for North America stations and observed prominent improvements

### Supporting Information:

Supporting Information may be found in the online version of this article.

### Correspondence to:

S. Shi,  
sshi2@fsu.edu

### Citation:

Shi, S., & Liu, G. (2024). Improvements on phase classification using atmospheric melting and refreezing energy based on soundings. *Journal of Geophysical Research: Atmospheres*, 129, e2023JD040030. <https://doi.org/10.1029/2023JD040030>

Received 18 SEP 2023

Accepted 22 APR 2024

### Author Contributions:

**Conceptualization:** Guosheng Liu  
**Data curation:** Shangyong Shi  
**Formal analysis:** Shangyong Shi  
**Funding acquisition:** Guosheng Liu  
**Investigation:** Shangyong Shi  
**Methodology:** Shangyong Shi  
**Project administration:** Guosheng Liu  
**Resources:** Guosheng Liu  
**Software:** Shangyong Shi  
**Supervision:** Guosheng Liu  
**Visualization:** Shangyong Shi  
**Writing – original draft:** Shangyong Shi  
**Writing – review & editing:**  
Guosheng Liu

## Improvements on Phase Classification Using Atmospheric Melting and Refreezing Energy Based on Soundings

Shangyong Shi<sup>1</sup>  and Guosheng Liu<sup>1</sup> 

<sup>1</sup>Department of Earth, Ocean and Atmospheric Science, Florida State University, Tallahassee, FL, USA

**Abstract** Determining precipitation as solid (snow) or liquid (rain) phase is crucial for remote sensing of precipitation. Most phase classification methods rely on near-surface temperatures. Further attempts to incorporate atmospheric information aloft only achieved mixed level of success, particularly for precipitation with temperature inversion. In our study, we developed a phase classification scheme based on the upper-level melting energy (ME) and refreezing energy (RE), which is proportional to the area enclosed by the temperature profile and the 0°C isotherm. We performed least squares fitting and linear discriminant analysis to derive phase separation functions using observed surface and sounding data in North America. We provided separation functions for snow conditional probabilities ranging from 30% to 80% for various applications. Compared to a previously published (Probsnow) method, our energy method achieved comparable performance for Type 1 soundings with one near-surface melting layer, and significantly improves the phase classification scores for Type 2 soundings with an aloft melting layer and a near-surface refreezing layer. We innovatively combined surface ice-bulb temperature with the ratio between the ME and RE to represent Type 2 profiles. For Type 2 soundings, our energy method improves the Heidke skill score (HSS) from 0.25 to 0.47 and reduces false alarm rate (FAR) by 0.47 compared to the Probsnow method for 50% threshold. By applying the physically based method, we improved accuracy and HSS, and reduced FAR for more than two thirds of the evaluation stations across the North America. Finally, we tested the application of the new method in satellite snowfall retrievals.

**Plain Language Summary** In this study, we developed a method to determine whether precipitation is in the form of snow or rain, which is important for weather forecast, modeling, and snowfall measurements with radar. We used atmospheric melting and refreezing energy to represent the physical process that falling precipitation undergoes. Two types of atmosphere structures were considered: melting near the surface (Type 1), and melting-refreezing profiles (Type 2). Compared to a previous method, we achieved comparable performance for the Type 1 soundings, and achieved major improvements for the Type 2 soundings, where the process of melting and refreezing was not well-represented by previous methods. Our new method was tested in North America and showed improvements in most stations. The improvements in phase prediction for Type 2 soundings contribute significantly to the overall phase classification for most stations in the North America. Finally, we tested our method for satellite snowfall retrievals. For future applications, we offer different separation functions for various thresholds of the conditional probability of snow to meet different prediction needs.

## 1. Introduction

Knowing surface precipitation phase is crucial for hydrological and satellite remote sensing studies. Past studies have analyzed the long-term trend of the phase partitioning in the Northern Hemisphere, and decreases in the snow to total precipitation ratio are commonly observed (Dettinger et al., 2015; Fassnacht et al., 2016; Feng & Hu, 2007; Han et al., 2018; Irandoust et al., 2017; Knowles et al., 2006; Serquet et al., 2011; Shi & Liu, 2021; J. Wang et al., 2016). Changes in precipitation phase affect snow accumulation and snowmelt timing (Clow, 2010), thus influence streamflow prediction (Barnhart et al., 2016; Berghuijs et al., 2014; Ellis & Sauter, 2017). In satellite precipitation retrievals, different precipitation phases correspond to different relations to be used to convert radar reflectivity to precipitation rate (Liu, 2008). Although remote sensing instruments, especially spaceborne ones, have become vital hydrological monitoring tools, they are often unable to correctly classify precipitation phase themselves (Maahn et al., 2014). Ground-based observations or model-derived thermodynamic fields are then needed to provide guidance (Pettersen et al., 2021). Therefore, developing an algorithm for phase classification based on ancillary atmospheric data is of great importance.

Most state-of-the-art phase classification methods rely on simple algorithms developed from surface temperatures, ranging from a single or a combination of temperature thresholds to statistical functions of temperatures (Dai, 2008; Ding et al., 2014; Fassnacht et al., 2013). Heymsfield et al. (2021) showed that snow can reach the surface at temperatures as warm as 5°C. Therefore, the temperature threshold for classifying snow and rain varies from -5 to 6°C depending on locations, while it mostly falls between 0°C and 1°C (Jennings et al., 2018; Sims & Liu, 2015). Further studies based on dewpoint temperature (Marks et al., 2013; Ye et al., 2013), wet-bulb temperature ( $T_w$ ) and ice-bulb temperature ( $T_i$ ) (Heymsfield et al., 2021) have shown that using variables that contain moisture information in the phase classification would improve the prediction performance.

Nevertheless, surface information alone is not adequate for phase classification. Sims and Liu (2015) found that for the southeastern coast of the continental United States,  $T_w$  needs to be lower than 0°C for snowfall; for the western mountainous area, precipitation maintains in solid phase even if  $T_w$  is warmer than 2°C. The atmospheric profile was believed to contribute to such differences. A typical process for snow to be observed is: ice and snow crystals form in clouds, grow by deposition, riming and aggregation, fall through the atmosphere, and stay in solid phase until they reach the surface. Therefore, the falling process needs to be emphasized when determining precipitation phase either explicitly by microphysics schemes or implicitly by vertical thermal profiles, which forms another major category of phase classification scheme that incorporates atmospheric information. In this study, we chose to develop the phase classification scheme using in situ observations where the precipitation phase and the vertical atmospheric structure are concurrently recorded at weather stations (Harpold et al., 2017). The precipitation phase classification scheme of Sims and Liu (2015) was also intended at least partially to include information on atmospheric vertical structures, and we will introduce it later in this chapter. Since it has been implemented in several satellite precipitation retrieval algorithms (Huffman et al., 2020; Kubota et al., 2020; Randel et al., 2020), in this study we will use the Sims and Liu scheme as a reference, and assess the performance of the newly developed scheme against it.

Figure 1 shows four common types of atmospheric temperature profiles for precipitation events depending on how the profile intersects with the 0°C isotherm (Birk et al., 2021; Bourgouin, 2000; Feicabruno et al., 2015; Thériault et al., 2006). When the entire atmosphere below a certain height is below freezing (Type 0A) or above freezing (Type 0B), snow or rain would occur, respectively. If the profile crosses the 0°C isotherm one or more times, it indicates the presence of atmospheric layers experiencing above or below freezing temperatures, referred to as melting or freezing layers. When there is a melting layer warmer than 0°C above the surface (Type 1), rain and/or snow is possible depending on the melting layer depth. If solid particles fall through a melting layer aloft and followed by a refreezing layer underneath (Type 2), the phase when reaching surface depends on the competition between the extents of melting and refreezing processes. Snow is likely to occur when the melting layer is shallow enough compared to the refreezing layer. Freezing rain and/or ice pellets are also possible for Type 2 soundings. Though various types of solid precipitation can be observed, we chose to focus only on snow (solid) and rain (liquid). One reason is to keep the precipitation categorization identical to Sims and Liu (2015) to ensure fair comparison. The other important reason is the difficulty to separate freezing rain from rain with current observation data, which we will discuss in the methodology section.

These atmospheric profiles partially explain the misclassification of precipitation events by using single temperature thresholds. For Type 1 soundings, if the melting layer is thin, the snow particles fall fast through the layer and may maintain solid form when reaching the ground, thus snow would be observed at warmer surface temperatures, which is possibly the cause for the underestimation of number of snow events. For Type 2 soundings, even if the surface is cold enough, the precipitation phase at the surface may still be liquid due to the temperature inversion and melting aloft. This may lead to the overestimation of conditional probability of snow (number of snow events over number of precipitation events) as seen in both Figures 2a and 2b.

The phase classification scheme developed by Sims and Liu (2015) intended to include atmospheric information by using the lapse rate of the lowest 500 m. With the input of surface wet-bulb temperature and low-level lapse rate calculated from temperature profiles, the conditional probability of snow would be predicted through a look-up table. A probability of less than 50% is assigned to be rain event, otherwise snow. This method, referred to as “Probsnow” hereinafter, has a good performance in reducing the mean bias in snow conditional probability estimation to 2% (Figure 2c) compared to using single temperature or wet-bulb temperature threshold (Figures 2a and 2b). The reason for such improvement is that the combination of surface temperature and low-level lapse rate accounts for some of the effects by the warm layer above the surface as shown in Type 1 soundings. However, it

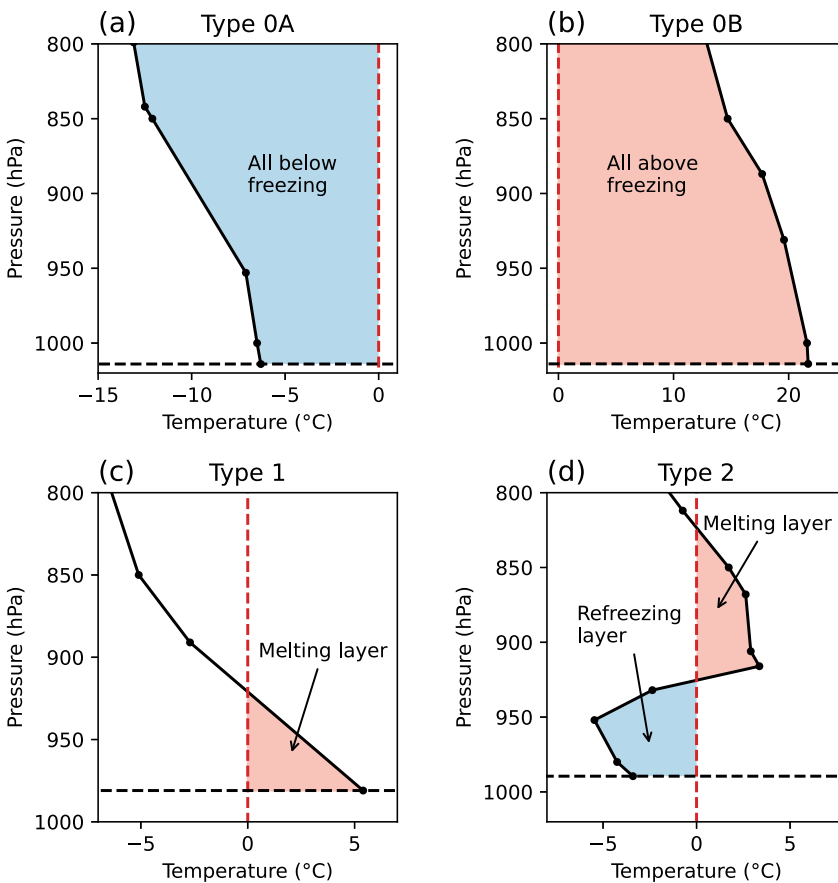


**Figure 1.** Common sounding types for precipitation events.

does not take into account the complicated temperature profile for Type 2 soundings. Many rain events could have been misclassified as snow due to the below-freezing surface temperature. As shown in Figure 3, aside from Type 0 soundings, for most stations, more than 50% of snow events belong to Type 1 and the remaining 20%–40% belong to Type 2 soundings. Type 2 soundings play an important role in snow events, particularly in the central to eastern United States, where the majority of cold season precipitation occurs with cold fronts (Catto et al., 2012). Considering the significant presence of Type 2 soundings in snow events, correctly classifying precipitation phase for Type 2 soundings would greatly enhance our prediction skills. Therefore, a more sophisticated variable is needed to represent the two-layer atmospheric structure to improve phase prediction for Type 2 soundings.

A number of studies have explored the skills of different upper-level atmospheric variables in determining precipitation phase, such as the freezing level height (Pandolfo, 1957), 1,000–700 hPa thickness (Murray, 1952), lapse rate (Froidurot et al., 2014), etc. The approach using atmospheric energy stands out with its physical basis and simplicity. The atmospheric energy is defined to be proportional to the area between the  $0^{\circ}\text{C}$  isotherm and the temperature profile in the warm/cold layer, and can be estimated as the product of the mean temperature and the depth of the layer (Bocchieri, 1980; Iribarne & Godson, 1973). Bourguin (2000) first developed a classification method based on the energy, and Birk et al. (2021) further improved the method by increasing the sample size, switching to wet-bulb temperature profile rather than temperature, and refining the fitting. The revised Bourguin method provides probabilities of various types of precipitation including freezing rain, ice pellets, rain, snow, and their combinations. Though the method exhibits good performance, it put more emphasis on the mixed-type precipitation and did not specifically separate snow from the discussion. Therefore, it is not applicable to snowfall retrieval problems where an output of either solid or liquid form is expected.

Based on the idea of atmospheric energy, we developed a scheme, referred to as the energy method, for classifying between liquid (rain) and solid precipitation (snow) with the intention to achieve a balance between accuracy and simplicity. Additional emphasis is drawn to the Type 2 soundings, which the Probsnow method struggles with. By

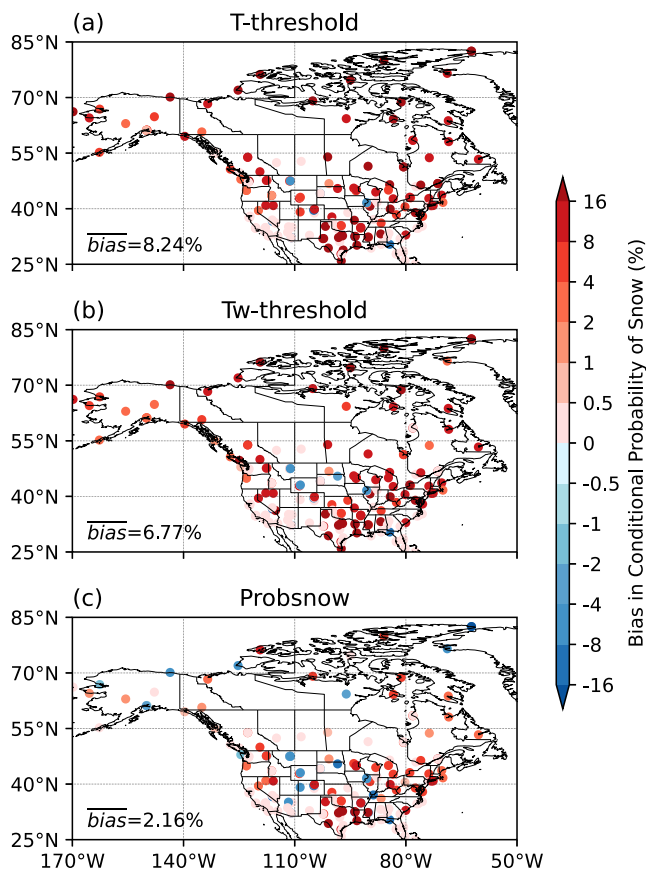


**Figure 2.** Bias in conditional probability of snow estimated by (a) temperature threshold of  $2^{\circ}\text{C}$ , (b) wet-bulb temperature threshold of  $1^{\circ}\text{C}$ , (c) Probsnow scheme with inputs of surface wet-bulb temperature and temperature lapse rate. The conditional probability of snow is calculated as the number of snow events divided by the number of precipitation events.

Sounding data are from Integrated Global Radiosonde Archive (IGRA) data set (Durre et al., 2016). Vertical profiles of temperature and relative humidity along with geopotential heights and pressures were collocated with

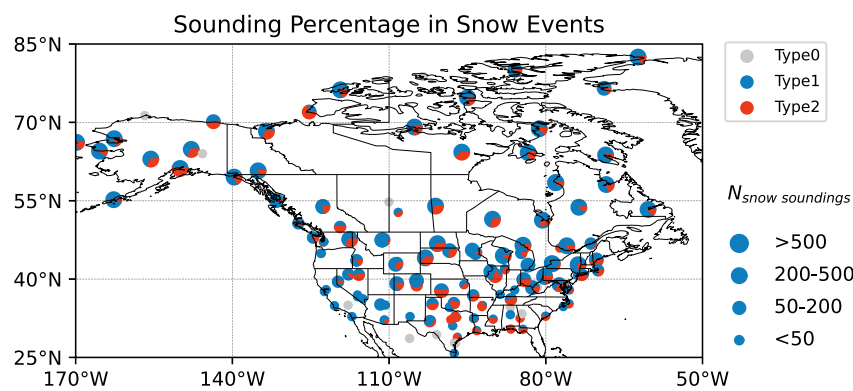


**Figure 3.** The percentage of Type 1 (blue) and Type 2 (red) soundings in snow events. The profile of ice-bulb temperature is used to identify the sounding types. Type 0 soundings are excluded from the percentage calculation. Only when all snow events belong to Type 0, a full gray pie chart would be presented. The size of pie charts indicates number of available soundings at the station.

better representing the atmospheric vertical profiles, we aim at improving the phase classification scores for Type 2 soundings, thus improving the overall phase prediction performance. This scheme would be useful for problems that require an input of solid or liquid precipitation phase, such as satellite precipitation retrievals, phase determination in reanalysis data, or climate predictions. The data preparation is described in Section 2. In Section 3, we explore the performances of adopting different temperature-related variables, and present the development of energy method for Type 1 soundings. In Section 4, we go through the development of phase classification functions for Type 2 soundings, and discuss in detail about the improvements and limitations of the energy method. In Section 5, we evaluate the performance of the energy method compared to the Probsnow method, and present the difference the energy method would make in satellite snowfall retrievals. Section 6 concludes the study with a summary of key points and a discussion.

## 2. Data Preparation

### 2.1. Training and Evaluation Data Sets

We used the National Centers for Environmental Prediction (NCEP) Automated Data Processing (ADP) operational global surface observations to obtain near-surface atmospheric variables and precipitation phase. Two data sets, ds464.0 from January 1978 to February 2007 (<https://rda.ucar.edu/datasets/ds464.0/>) and ds461.0 from February 2007 to December 2019 (<https://rda.ucar.edu/datasets/ds461.0/>), were merged to create a longer series following Shi and Liu (2021). Variables used include near-surface temperature, dew point temperature, surface pressure, and the present weather codes ("ww" codes). Reported by human observers, the present weather codes indicate the weather phenomenon at the time of observation. If there are multiple weather phenomena, only those with larger ww codes would be reported. Following the definition in Sims and Liu (2015), we considered two major precipitation categories: solid (snow) and liquid (rain), that is, ww codes 70–79, 85 and 86 being categorized as snow, and ww codes from 60 to 99 except for those snow codes above being categorized as rain. Freezing rain and mixed precipitation were assigned to the rain category.

surface observations in NCEP ADP. Weather station data that have collocated IGRA sounding within  $0.25^{\circ}$  (longitude)  $\times 0.25^{\circ}$  (latitude) at the same observation hour were used to generate the training and the evaluation data set. If there was more than one sounding matched with surface stations, only the nearest one was kept as matchup data. The spatial distribution of the stations can be seen in Figure 3. After categorizing the soundings into Type 0, Type 1 and Type 2, we randomly selected 80% data for training and the rest 20% for evaluation.

The near-surface values and vertical profiles of wet-bulb and ice-bulb temperatures were calculated from temperature, relative humidity and pressure with Newton's iteration method (see Text S1 in Supporting Information S1).

## 2.2. Data Cleaning

Occasionally, the surface temperature may differ from the temperature at the lowest level (typically less than a couple of meters) of the collocated sounding. We discarded the data if the difference in the temperature between the surface and the lowest level of the sounding is larger than  $2^{\circ}\text{C}$ , or the surface temperature is below freezing when the lowest level of the sounding is above-freezing. Such data cleaning would avoid unrealistic values in the following calculation of the energy.

## 2.3. Energy Definition

Bourgouin (2000) suggested that the mean temperature of a layer and the layer height are critical to phase diagnosis, and their product forms a predictor proportional to the area between the  $0^{\circ}\text{C}$  isotherm and the environment temperature on tephigrams, shown as the shaded area in Figures 1c and 1d. A melting layer warmer than  $0^{\circ}\text{C}$  has a positive area indicating melting energy (ME), and a refreezing layer has a negative area indicating refreezing energy (RE). These energies can be estimated by the method of the mean adiabat:

$$\text{Energy area} = C_p |\text{area}| = R_d \bar{T} \ln\left(\frac{p_{\text{bottom}}}{p_{\text{top}}}\right), \quad (1)$$

where  $\bar{T}$  is the mean relative (to  $0^{\circ}\text{C}$ ) temperature of the layer,  $C_p$  is the specific heat at constant pressure and  $R_d$  is gas constant for dry air. The  $p_{\text{bottom}}$  and  $p_{\text{top}}$  are the pressure at the bottom or top of considered layer. Negative values indicate layers colder than  $0^{\circ}\text{C}$ , but we will refer its absolute value to as RE for simplicity. For each melting or refreezing layer, we applied Equation 1 to each neighboring ( $T, p$ ) data pairs and integrated the result to get the energy for the entire layer. The energies were calculated for the collocated soundings up to 2 km above the surface. For more detailed description of the integral, please refer to Text S2 and Figure S1 in Supporting Information S1.

More than 330,000 soundings from 1978 to 2019 were collocated with NCEP ADP stations. We categorized them into Type 0, Type 1 and Type 2 according to the vertical structure (Figure S2 in Supporting Information S1). For Type 1 soundings, there are more than 38,000 soundings in the training set and more than 9,600 soundings in the evaluation set. There are 2,092 and 523 Type 2 soundings in the training and evaluation sets, respectively. The sample size of Type 2 soundings is 6 times of that in Birk et al. (2021).

## 2.4. Conditional Probability of Snow

We used the conditional probability of snow to evaluate phase transition throughout our study. The conditional probability of snow, or “snow probability,” is calculated as the number of snow events divided by number of precipitation (rain and snow) events. It depicts the probability for snow to occur when there is precipitation. A conditional probability of 50% for snow events is commonly used as the separation between solid and liquid precipitation (e.g., Auer, 1974; Jennings et al., 2018; Sims & Liu, 2015). The meaning is similar to “50% chance of snow” or “50% accurate at predicting snow” when it is precipitating. Since 50% is not the only option for various applications, we provide separation functions for conditional probabilities of snow from 30% to 80% with 10% increment for readers to choose from. Users would be able to determine the precipitation phase with the input of surface ice-bulb or wet-bulb temperature and the vertical temperature and relative humidity profiles.

## 2.5. Satellite Application

We examined how much a difference our energy method would make compared to the Probsnow method in satellite snowfall retrievals as application of the method. The CloudSat 2B-GEOPROF R05 radar reflectivity product for year 2008 (Marchand et al., 2008) is used. We excluded noisy surface echoes by neglecting the first six bins above the surface (around 1.5 km). Uncontaminated reflectivities larger than  $-10$  dBZ were considered as precipitation. The fifth generation European Centre for Medium-Range Weather Forecasts Reanalysis (ERA5) hourly data on pressure levels (Hersbach et al., 2023a) and single level (Hersbach et al., 2023b) were matched with satellite observations to provide temperature and moisture profiles. When precipitation occurs, the precipitation phase was determined by the newly developed energy and the Probsnow methods. When snow was predicted, we used the relation proposed by Liu (2008),  $Z = 11.5S^{1.25}$ , to convert radar reflectivity  $Z$  into snowfall rate  $S$ , where  $Z$  is in the unit of  $\text{mm}^6\text{m}^{-3}$ , and  $S$  has the unit of  $\text{mm h}^{-1}$  (liquid-equivalent).

## 2.6. Evaluation Metrics

The performance of the classification was evaluated using five metrics: accuracy, probability of detection (POD), false alarm rate (FAR), Heidke skill score (HSS) and true skill statistics (TSS). All the metrics were calculated from a 2 by 2 contingency table (Table S1 in Supporting Information S1). Following the advice from Barnes et al. (2009), here we clarify the calculation of the FAR to avoid confusion with the term “false alarm ratio.” The FAR could be regarded as “probability of false detection” mirroring the definition of POD. It is calculated as the number of false snow events divided by the number of observed rain events, which equals the sum of false snow and true rain. The ranges for accuracy, HSS and TSS are  $[0, 1]$ ,  $[-1, 1]$  and  $[0, 1]$ , respectively, and values closer to 1 indicate better overall prediction performance. Detailed definitions and calculations are shown in Text S3 of Supporting Information S1.

# 3. Classification for Type 1 Soundings: Near-Surface Melting Layer

## 3.1. Wet-Bulb Temperature and Ice-Bulb Temperature

As introduced before, incorporating moisture in the phase classification will improve the prediction performance (Figures 2a and 2b). The wet-bulb temperature, measured by a thermometer with moistened bulb, takes into account the evaporational cooling to the liquid surface (Penn, 1957), while the ice-bulb temperature considers the sublimation or melting of an ice surface. In our discussion about the Type 1 and Type 2 soundings, we are mostly dealing with the melting and freezing of frozen particles unless it is completely melted. Therefore, it is the ice-bulb temperature that better represents the temperature for the falling hydrometeor (Heymsfield et al., 2021), and we based our analysis on  $T_i$ . Since the difference between  $T_w$  and  $T_i$  is small when the air is close to water saturation, we also conducted identical analysis with  $T_w$  and would provide the phase classification function coefficients for the users to choose from.

## 3.2. The Classification Function for Type 1 Soundings

We first explored the relationship between ME and the conditional probability of snow events. From a physical perspective, when there is only one melting layer near the surface, whether the falling hydrometeor would completely melt when reaching the surface depends on how much energy this layer provides. For a fixed surface temperature, the value of ME can differ greatly with varying lapse rate. Thus, for Type 1 profiles, the use of ME would be a better option than using surface temperature alone.

We computed the ME based on temperature, wet-bulb temperature and ice-bulb temperature profiles. We calculated the conditional probability of snow for every 2 J/kg of ME, and the results are shown in red dots in Figure 4. We observed a clear exponential decrease of the snow conditional probability with the increase of ME. To derive a ME threshold for phase change, we fitted with an exponential function in the form of  $F(x) = \alpha \exp(-\beta x) + 1 - \alpha$ , where  $\alpha$  and  $\beta$  are fitting coefficients, and  $x$  is ME calculated from either  $T$ ,  $T_w$  or  $T_i$ , denoted as TME, TwME, or TiME. The function is consistent with our definition of ME as the snow conditional probability approaches one when the ME approaches zero. The fitted conditional probability of snow with ME is shown in Figure 4.

For temperature-based ME (TME), the threshold of 50% conditional probability of snow is 5.5 J/kg (Figure 4a), and for wet-bulb temperature based ME (TwME) and ice-bulb temperature based ME (TiME), the threshold is

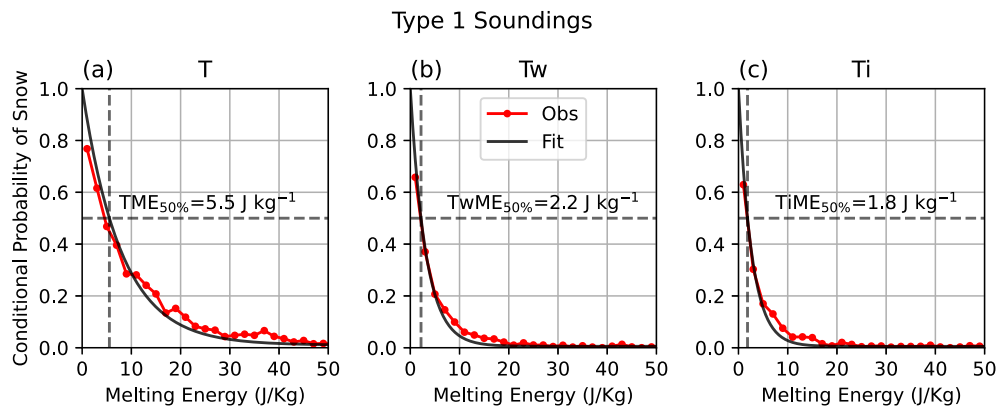


**Figure 4.** Conditional probability of snow with respect to melting energy (ME) calculated with (a) temperature (TME), (b) wet-bulb temperature (TwME) and (c) ice-bulb temperature (TiME) profiles for Type 1 soundings. Red dots are observed values and the black line shows fitted exponential function in the form of  $F(x) = \alpha \exp(-\beta x) + 1 - \alpha$ , where  $\alpha$  and  $\beta$  are fitting coefficients. The ME thresholds ( $TME_{50\%}$ ,  $TwME_{50\%}$ ,  $TiME_{50\%}$ ) shown in the legends are the energies where the conditional probability of snow reaches 0.5 (dashed lines).

2.2 J/kg and 1.8 J/kg, respectively (Figures 4b and 4c). The precipitation events with ME smaller than the threshold would be recognized as snow. As shown in Table 1, compared to the Probsnow classification scheme, the TME method achieves similar accuracy but slightly lower HSS and TSS score, while the TwME and the TiME thresholds achieves the same POD and comparable accuracy, HSS and TSS. The better performance of Tw compared to temperature in phase partitioning is consistent with previous studies (e.g., Behrang et al., 2018; Booth, 1973; Ding et al., 2014; Lumb, 1961, 1963; Sims & Liu, 2015; Y.-H. Wang et al., 2019). The difference between using TwME and TiME is small and does not influence our decision on using Ti for the rest of the study.

### 3.3. Improved Classification Function for Type 1 Soundings

The results in Section 3.2 led us into wondering if any further improvements can be made for Type 1 soundings. Given the same ME, surface temperature could be different depending on the lapse rate, which corresponds to different falling time in the melting layer. In contrast, as we introduced earlier, the Probsnow method well classifies precipitation phase for Type 1 soundings since the surface temperature and lapse rate well represent the atmospheric profile. Therefore, we further considered combining surface temperature and low-level ME in classifying precipitation and refer it as Ti + TiME hereinafter.

The scatter plot of rain and snow events based on Ti and TiME is shown in Figure 5a. The precipitation events scatter diagonally, and most snow events are observed at  $Ti < 1.5^\circ\text{C}$  and  $TiME < 3 \text{ J/kg}$ . We computed the running mean of conditional probability of snow for each Ti bin of  $0.5^\circ\text{C}$  and TiME bin of  $1 \text{ J/kg}$  (detailed method in Text S4 of Supporting Information S1) and show the contour map in Figure 5b. The probability of snow decreases with increasing TiME at fixed surface Ti, which corroborates the idea of Sims and Liu (2015) that lapse rate would affect the phase changes by altering the time of a hydrometeor falling through the melting layer. For a fixed surface Ti, a larger ME corresponds to a larger lapse rate, longer time in the melting layer, and thus more melting of the hydrometeor.

Based on Figure 5b, for the Type 1 soundings, we defined the classification function as:

$$S_1 = Ti - a \exp(b TiME), \quad (2)$$

where  $a$  and  $b$  are fitting coefficients (see Text S4 in Supporting Information S1 for details about the fitting). The phase decision will be snow if  $S_1$  is

**Table 1**

*Classification Metrics by the Probsnow Method and the New Energy Method for 50% and 70% Snow Conditional Probabilities<sup>a</sup>*

		Accuracy	POD	FAR	HSS	TSS
50%	Probsnow	0.95	0.66	0.027	0.64	0.64
	Energy	0.94	0.53	0.026	0.55	0.51
	TME	0.95	0.66	0.031	0.62	0.63
	TwME	0.94	0.66	0.033	0.61	0.63
70%	Ti + TiME	0.96	0.65	0.02	0.65	0.63
	Probsnow	0.94	0.26	0.004	0.37	0.25
	Energy	0.95	0.37	0.007	0.48	0.36

<sup>a</sup>TME/TwME/TiME refers to adopting single melting energy thresholds calculated from T/Tw/Ti profiles for the classification (5.5/2.2/1.8 J/kg). Ti + TiME refers to adopting the separation function derived from the dependence of snow conditional probability on both Ti and TiME. The coefficients for the separation functions can be found in Table 2. The Ti + TiME method is adopted in our final scheme. Probsnow method by Sims and Liu (2015) uses inputs of surface wet-bulb temperature and lapse rate calculated from temperature profiles.

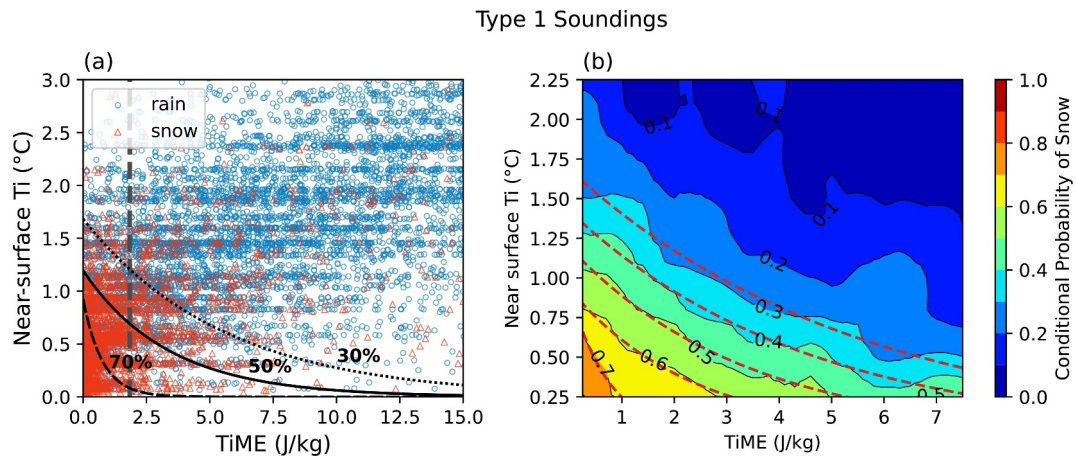


**Figure 5.** (a) Scatter plot of rain (blue circles) and snow (red triangles) events with Type 1 soundings with respect to TiME and near-surface  $T_i$ . The derived separation boundary (snow conditional probability of 50%) is shown in black, solid line. The separation lines for snow conditional probability of 30% and 70% are shown in black dotted and black dashed lines. The single TiME threshold of 1.8 J/kg derived in Figure 4c is shown in gray, dashed line. (b) Contour map of snow conditional probability calculated from (a) that is used to derive the separation functions. Red dashed lines are the fitted exponential functions in the form of  $T_i - a\exp(b \text{TIME}) = 0$ , where  $a$  and  $b$  are coefficients summarized in Table 2.

less than 0, otherwise rain. The fitted exponential functions for all available snow probability are plotted in Figure 5b, with the coefficients shown in Table 2. Though we haven't had a theoretical base for the relationship, we adopted the exponential function because the R-squared scores for the exponential models exceeds 0.96 for snow conditional probability larger than 30% and outweigh the scores for linear models for up to 0.1.

We evaluated the performance of the classification function (Equation 2) using 50% and 70% snow probability thresholds. Compared to the TiME alone threshold method (50%), combining  $T_i$  and TiME achieves higher accuracy and HSS, and lower FAR (Table 2). This improvement can be seen more straightforwardly in Figure 5a by comparing the thick gray dashed vertical line, which is the  $\text{TiME} = 1.8 \text{ J/kg}$  threshold, with the black solid separation line for 50% snow conditional probability. The single TiME threshold regards all events to the left of the gray line as snow, while the  $T_i + \text{TiME}$  combined method correctly captures rain events with moderate ME and warm  $T_i$  (above the black exponential line, to the left of the gray line), thus reducing false alarms for snow and increasing accuracy score. The combined method also correctly identifies snow events with moderate ME and cold surface  $T_i$ .

Since our method and the Probsnow both address the presence of the near-surface melting layer with different variables, it is expected that the two methods have comparable performances for Type 1 soundings. The performance of the combined method is similar to the Probsnow method for the 50% snow probability (HSS score of 0.65 vs. 0.64), but exceeds Probsnow for the 70% snow probability in case of POD, HSS and TSS.

**Table 2**  
Coefficients of the Separation Function (Equation 2) for Type 1 Soundings With Different Conditional Probabilities of Snow<sup>a</sup>

Probability of snow	$T_i$		$T_w$	
	$a$	$b$	$a$	$b$
30%	1.7	-0.18	1.8	-0.17
40%	1.4	-0.22	1.6	-0.21
50%	1.2	-0.30	1.3	-0.27
60%	0.93	-0.43	1.0	-0.36
70%	0.92	-1.3	0.73	-0.45

<sup>a</sup>Snow is predicted if  $S_1 < 0$ . Results based on  $T_i$  and  $T_w$  are shown. We adopted the  $T_i$ -based coefficients in our study.

## 4. Classification for Type 2 Soundings: Melting and Refreezing Layers

### 4.1. Limitation of Previous Methods

Section 3 has shown that energy can be used to represent atmospheric structure in phase classification. Therefore, we continued to explore the application of the energy in Type 2 soundings. There are 2,092 soundings in the training and 523 soundings in the evaluation data for Type 2 soundings in our study, far exceeding the sample size in Bourguin (2000) and Birk et al. (2021) (119 and 242, respectively). From previous discussions, the precipitation phase would depend on the contribution of the melting and refreezing layers, that is, the ME and RE. Figure 6 shows the TiME and TiRE of rain and snow events in Type 2 soundings. Most snow events have TiME smaller than 50 J/kg, and most rain events have TiRE smaller than 100 J/kg.

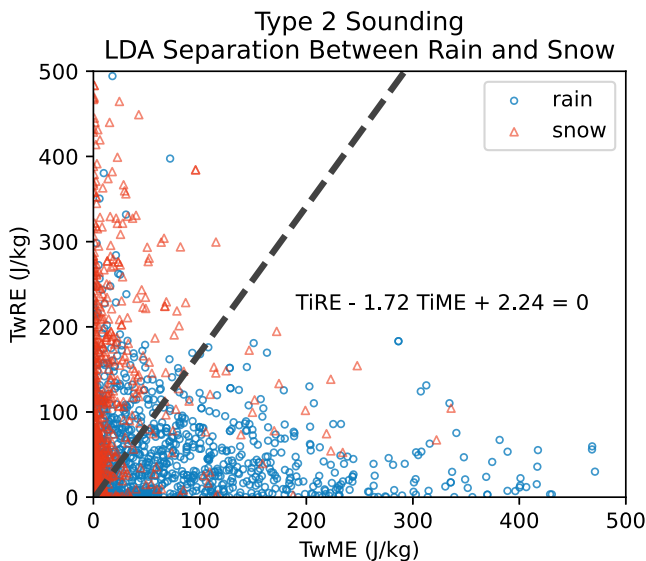


**Figure 6.** Rain and snow events in Type 2 soundings. The black dashed line is the boundary line of the linear discriminant analysis indicating the best separation between the two categories.

separation function (approximately 1.5) to create a new variable—the energy ratio. This ratio, denoted as  $3\text{TiME}/2\text{TiRE}$ , helps capture the balance between melting and refreezing effects. In Figure 6, the events with an energy ratio smaller than 1 are regarded as snow events. With the surface  $\text{Ti}$  and the energy ratio, we are able to better represent the melt-refreeze structure of Type 2 soundings.

Figure 7a presents the scatter plot of rain and snow events based on the energy ratio and surface  $\text{Ti}$ , with the energy ratio displayed on a logarithmic scale. There are events with  $\text{Ti}$  between 0 and  $1^\circ\text{C}$  in the Type 2 soundings since the extremely small melting near the surface would be neglected in the calculation (see caption for Figure S2 in Supporting Information S1). The line of  $\ln(3\text{TiME}/2\text{TiRE}) = 0$  corresponds to the black dashed line in Figure 6, and events to its right has larger contribution from melting than refreezing and vice versa. Most snow events fall in the third quadrant with negative  $\text{Ti}$  and negative log of energy ratio, indicating that lower temperature and more contribution of refreezing relative to melting are required to have snow events. In contrast, rain events dominate

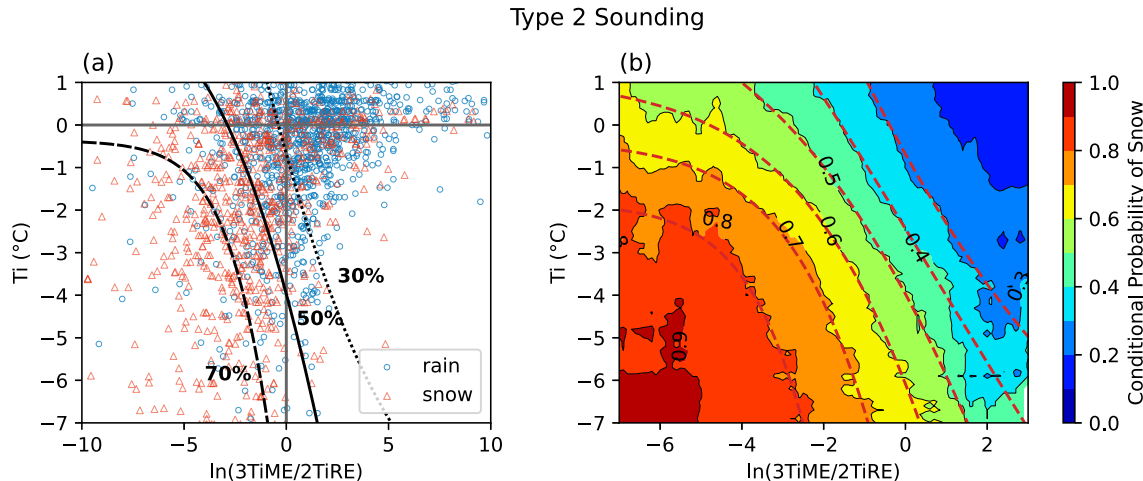


**Figure 7.** (a) Scatter plot of rain (blue circles) and snow (red triangles) events with Type 2 soundings with respect to the log of energy ratio  $\ln(3\text{TiME}/2\text{TiRE})$  and the surface ice-bulb temperature  $\text{Ti}$ . The fitted lines for the 30%, 50%, and 70% snow probability are shown in dotted, solid and dashed lines, respectively. (b) The contour map of snow conditional probability based on (a) that is used to derive the separation functions. Red dashed lines are the fitted hyperbolic tangent functions in the form of  $\text{Ti} + 18\tanh(c \times \ln(3\text{TiME}/2\text{TiRE}) + d) + e = 0$ , where  $c$ ,  $d$ , and  $e$  are coefficients summarized in Table 3.

To distinguish between rain and snow events, we initially conducted a linear discriminant analysis (LDA) and derived a separation boundary indicated by the black dashed line in Figure 6 following Birk et al. (2021). LDA is a common technique for reducing dimensionality and finding a linear transformation that discriminates different classes (Tharwat et al., 2017). Introduction of this method and how the boundary is defined can be found in Text S5 of Supporting Information S1. In regions where the LDA boundary  $S = 1.72 \text{TiME} - 2.24 - \text{TiRE} < 0$ , precipitation is categorized as snow and vice versa. However, the linear separation is less skillful due to the concentration of snow events with small  $\text{TiME}$  and  $\text{TiRE}$ , as well as the scarcity of data with both large energies. Birk et al. (2021) tried to improve the fitting by applying another LDA to the data with  $\text{ME} < 30 \text{ J/kg}$ , then composite a logarithmic fitting to the two LDA boundaries. But their determination of the cutoff threshold was somewhat arbitrary.

#### 4.2. Improved Phase Classification Function for Type 2 Soundings

We hope to derive the separation function from a more physically grounded approach. Similar to our approach for Type 1 soundings, we further introduced the surface ice-bulb temperature as an additional factor in the phase classification for Type 2 soundings to account for particle's falling time in the layers. Furthermore, taking into account the physical process of the competition between melting and refreezing, we leveraged the slope of the LDA

**Table 3**

Coefficients of the Separation Function (Equation 3) for Type 2 Soundings for Different Conditional Probabilities of Snow<sup>a</sup>

Probability of snow	Ti			Tw		
	c	d	e	c	d	e
30%	0.12	0.48	-7.40	0.32	0.11	0.50
40%	0.088	-0.064	3.59	0.28	0.24	-0.85
50%	0.14	-0.64	14.1	0.28	0.03	-3.5
60%	0.21	-0.69	16.9	0.31	0.14	-4.6
70%	0.30	-0.47	18.4	0.42	0.43	-6.1
80%	0.40	0.11	19.8	0.56	1.32	-7.3

<sup>a</sup>Snow is predicted if  $S_2 < 0$ . Results based on Ti and Tw are provided. We adopted the Ti-based functions in our analysis.

the first and the fourth quadrant. To provide a more precise description of the relationship, we generated a contour map depicting the running mean snow conditional probability (Figure 7b). The map exhibits a hyperbolic tangent-shaped pattern, with the conditional probability of snow increasing when the surface Ti gets colder and the energy ratio gets smaller, indicating a more profound refreezing layer near the surface.

For Type 2 soundings, we employed the separation function in the form of:

$$S_2 = Ti + 18 \tanh(cy + d) + e, \quad (3)$$

where  $c$ ,  $d$ , and  $e$  are coefficients, and  $y$  stands for the log of energy ratio  $\ln(3TiME/2TiRE)$ . The coefficient 18 was first obtained by fitting the 50% conditional probability line and subsequently applied to the other probability thresholds (30%–80%) to ensure consistent performance even when the variables fall out of boundaries. Further details on the methodology can be found

in the Text S6 and Figure S3 of Supporting Information S1. The coefficients for the snow conditional probability from 30% to 80% in an interval of 10% are shown in Table 3.

We evaluated the performances of Equation 3 when adopting thresholds of 50% and 70% and the results are shown in Table 4. When using the 50% threshold, although the POD decreased by 0.15, the FAR significantly reduced by 0.47, indicating stricter snow predictions. Overall, the energy method achieves higher accuracy, HSS and TSS compared to the Probsnow method. The accuracy is improved by 0.15 and the HSS score is improved by 0.22. Similar improvements are observed for the 70% threshold, with a higher HSS score with a remarkably low FAR of 0.05. When using a Tw based separation (coefficients shown in Table 3) derived from a slightly different data set, the TSS score increases from 0.26 to 0.49 for 50% threshold and from 0.34 to 0.36 for 70% threshold (not shown). Such improvements indicate that the combination of surface temperature, melting and RE improves the phase classification for Type 2 soundings significantly.

#### 4.3. Discussions on Type 2 Soundings

In Figure 8, we provide examples showcasing the vertical structure of different Type 2 sounding precipitation events. Notably, we observe that when the ME significantly outweighs the RE, rainfall is expected (as seen in Figure 8b), whereas dominance of the RE indicates snowfall (Figure 8c). However, instances such as those in Figures 8d and 8e, where the log of energy ratio is similar at approximately -0.1 yet precipitation phases differ, highlight the critical role of surface ice-bulb temperature. Warmer Ti conditions, coupled with a moderate energy ratio, favor a rain prediction (as demonstrated in example Figure 8d), while Ti below -5°C correctly classifies the event as snow (as evident in example Figure 8e). These examples emphasize the intricate interplay between melting and refreezing energies, along with surface temperature, in determining precipitation phase for Type 2 soundings.

Though the energy method for Type 2 soundings in the form of hyperbolic tangent function is derived from statistical computations to maximize R-squared score, it still has underlying physical meanings. Past studies only

use the combination of ME and RE, and we are the first to consider the relative contribution between the melting and refreezing and combine this ratio with surface temperature. We made these efforts to better represent the inversion profile of Type 2 soundings, proved by the significant improvements in the accuracy, HSS and TSS scores.

For a 50% threshold, the Probsnow method features extremely high POD of over 0.9 and a large FAR of 0.64. These two metrics indicate that, the Probsnow method tends to predict as many snow events as possible, which leads to many misclassifications of rain as snow (false alarm). This is the intrinsic limitation of the method. The median of the lapse rate of Type 2 soundings in the training data set is around 0.24°C/km. Large negative lapse rates of below -5°C/km are common indicating strong inversions. Based on the look-up table (Figure 4 in Sims and Liu (2015)), these events would mostly be classified as solid when temperature is below freezing. In contrast,

**Table 4**

Classification Performance Metrics for Type 2 Soundings for 50% and 70% Snow Conditional Probabilities<sup>a</sup>

		Accuracy	POD	FAR	HSS	TSS
50%	Probsnow	0.61	0.91	0.64	0.25	0.26
	Energy	0.74	0.76	0.17	0.47	0.46
70%	Probsnow	0.65	0.75	0.44	0.31	0.31
	Energy	0.68	0.36	0.05	0.33	0.32

<sup>a</sup>The energy method refers to the separation functions based on surface Ti and the ratio between melting and refreezing energy. The Probsnow method uses input of surface wet-bulb temperature and lapse rate calculated from temperature profiles.

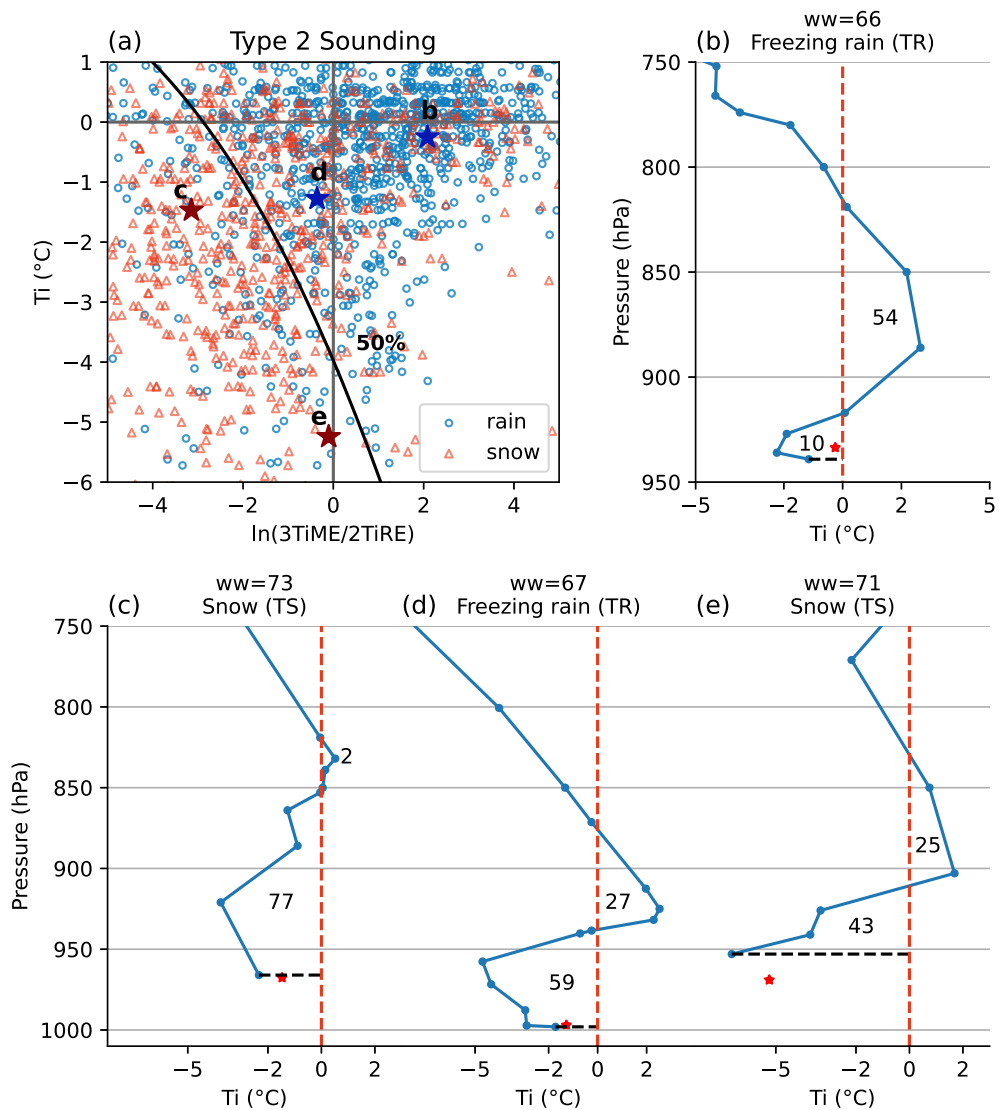


**Figure 8.** (a) A rescaled version of Figure 7, with the rain/snow examples marked with dark blue/dark red stars. (b–e) Example ice-bulb temperature profiles of Type 2 soundings. “ww” is the present weather codes from NCEP Automated Data Processing (ADP) observations, and TR, TS are abbreviations for true rain and true snow, indicating a correct prediction. The blue dots in (b–e) are the observations in IGRA soundings, while the red stars indicate the surface pressure and  $T_i$  observations from NCEP ADP weather stations. The numbers in the figure indicate the magnitudes of the melting or refreezing energy in the unit of J/kg.

our method achieves a high POD with much lower FAR, leading to a greatly improved HSS. We avoid “extreme” predictions of “almost all snow when temperature is below freezing” and achieve a more balanced prediction of rain and snow events.

After determining the phase as solid or liquid, we will be able to convert reflectivity measured by space-borne radars to snowfall or rainfall rates. More types of frozen precipitation, such as freezing rain, ice pellets and mixed precipitation are not specifically discussed in our study due to the mixture of different precipitation types and limited sample sizes. As shown in Figure S4 of Supporting Information S1, the freezing rain events mix with the rain events in the TiRE-TiME domain, making it difficult to separate freezing rain with rain in our training data set. Similarly, the spread of the ice pellets overlaps with that of snow events. Additionally, there are only 56 mixed precipitation events and 17 hail and thunderstorm events in our data set, which cluster at the lower left corner of the figure. It would be more challenging to classify these events considering the small sample size and rare occurrences.

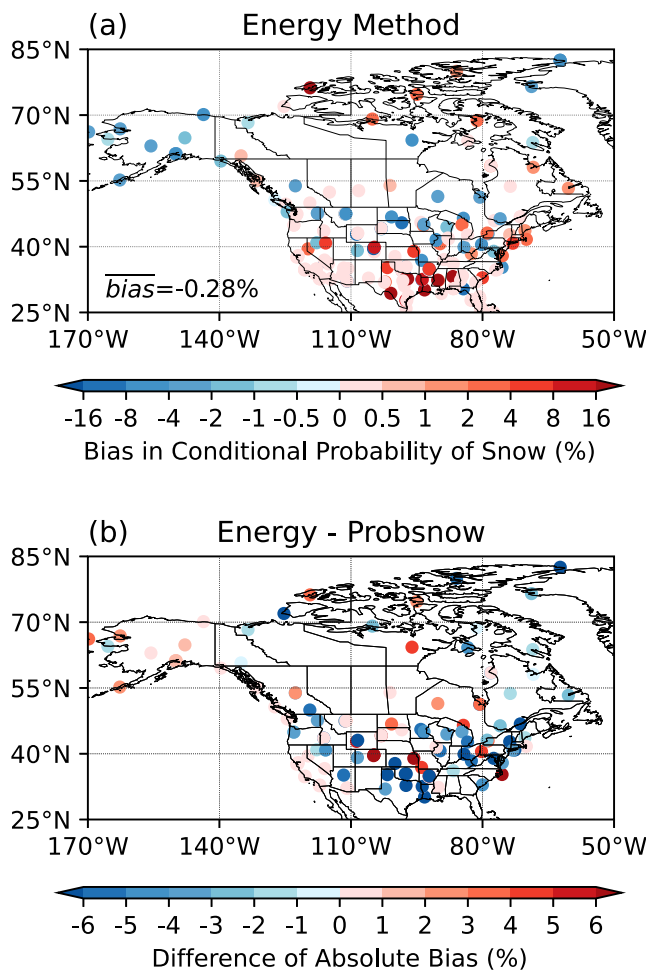


**Figure 9.** (a) Bias in snow fraction estimated by our energy method, and (b) the difference in the absolute bias in snow fraction of the energy method minus the Probsnow method.

of North America. Moreover, the accuracy is notably higher between 40° and 50°N and in eastern Canada. The HSS score, another metric for evaluating the overall performance, surpasses 0.6 for over two-thirds of the stations, reaching 0.8 for stations located in the mid-latitudes between 40° and 60°N. The POD exceeds 0.6 for the majority of sites. A higher POD with lower FAR would lead to more satisfying performance. While the POD is relatively lower at some stations in the western United States and Alaska, it is complemented by a notably small FAR in these regions.

Figure 11 illustrates the differences of the metrics when compared to the Probsnow method. Most stations show increased accuracy and HSS compared to the Probsnow method. Although the POD decreases slightly, there is a significant reduction in FAR as well, indicating a more balanced prediction which has been discussed in Section 4.2. Notably, these improvements persist when using a 70% threshold, as shown in Figure S7 of Supporting Information S1. The use of a 70% threshold leads to increased POD and reduced FAR for nearly all stations, with most stations east of 100°W featuring improved HSS and accuracy scores. Overall, the incorporation of physical processes into the phase classification enhances the scheme's performance.

## 5.2. Applications in Satellite Retrieval

We extended our evaluation to assess the impact of the energy method on satellite snowfall retrievals. Figure 12a illustrates the annual mean snowfall rate derived from CloudSat CPR data for the year 2008, with precipitation phase classified by the new energy method with a 50% threshold. Notable regions with substantial mean snowfall

There are more factors that influence the phase change of the falling hydrometeor. The ice particle could form in various shapes (e.g., columns, rosette, dendrite) and sizes with different terminal velocity and scattering properties (Liu, 2008). A lower pressure in mountains would result in the particle falling faster. However, current observations are still limited, and large uncertainty remains in the parameterization of the terminal velocity. Additionally, it would be informative to conduct idealized microphysics experiments to explore the extent of phase change in the melting or refreezing layer. However, since we are focusing on developing a statistical scheme, these would be out of the scope of this study.

## 5. Evaluation and Application

### 5.1. Station Performance Evaluation

We conducted a station-by-station evaluation of the new energy-based method using a 50% probability threshold. Performances of adopting a 70% probability threshold are shown in Figures S5–S7 of Supporting Information S1. Figure 9 illustrates the bias in conditional probability of snow introduced by the energy-based method, along with the difference in absolute bias when compared to the Probsnow method. In the southern United States, there are some stations where the bias magnitude exceeds 8%, while in the mid to high latitudes, the bias magnitudes remain within 4%. The mean bias for the energy-based method is  $-0.28\%$ , compared to  $2.16\%$  for the Probsnow method. As shown in Figure 9b, compared to the Probsnow method, a substantial reduction of over 5% is observed for some stations in the Rocky Mountains and mid- to eastern continental United States. Similar reductions in absolute bias are also evident in eastern and northern Canada. As indicated in Figure 3, these regions with less bias in snow conditional probability also exhibit a higher proportion of Type 2 soundings, reaffirming the enhanced performance of the energy-based method in classifying precipitation phase for Type 2 soundings.

Figure 10 displays the accuracy, HSS, POD and FAR of the energy method with a 50% threshold. The accuracy, which reflects the ability to correctly predict both rain and snow, consistently exceeds 95% along the Pacific coast

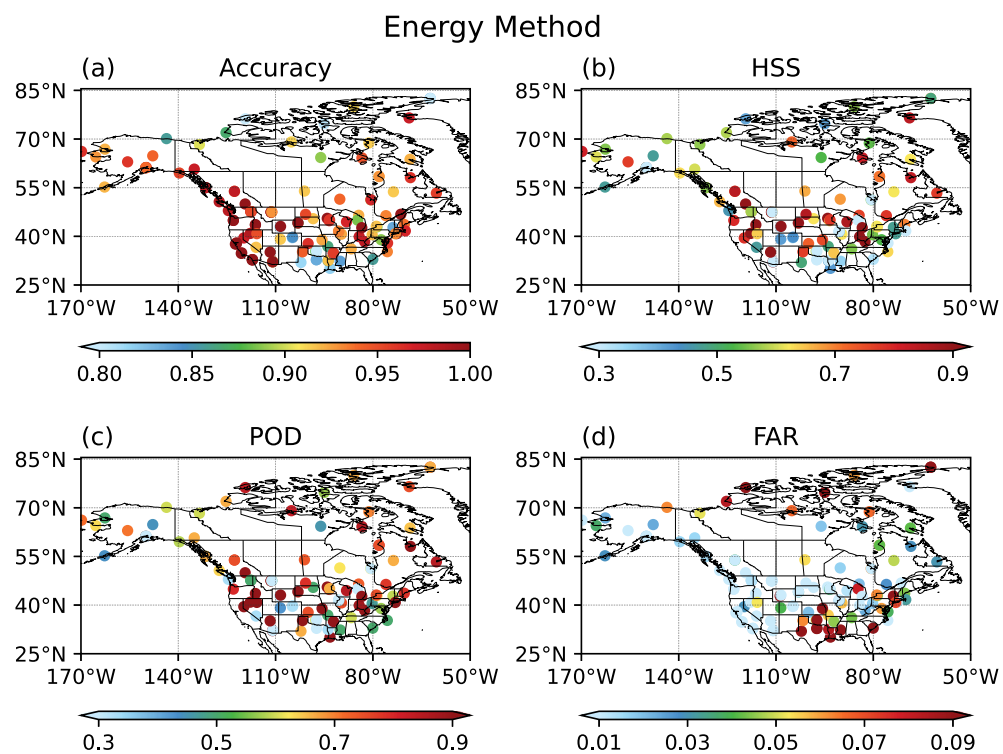


**Figure 10.** Classification metrics of the energy method using a threshold of 50%. (a) Accuracy, (b) Heidke skill score, (c) probability of detection, and (d) false alarm rate.

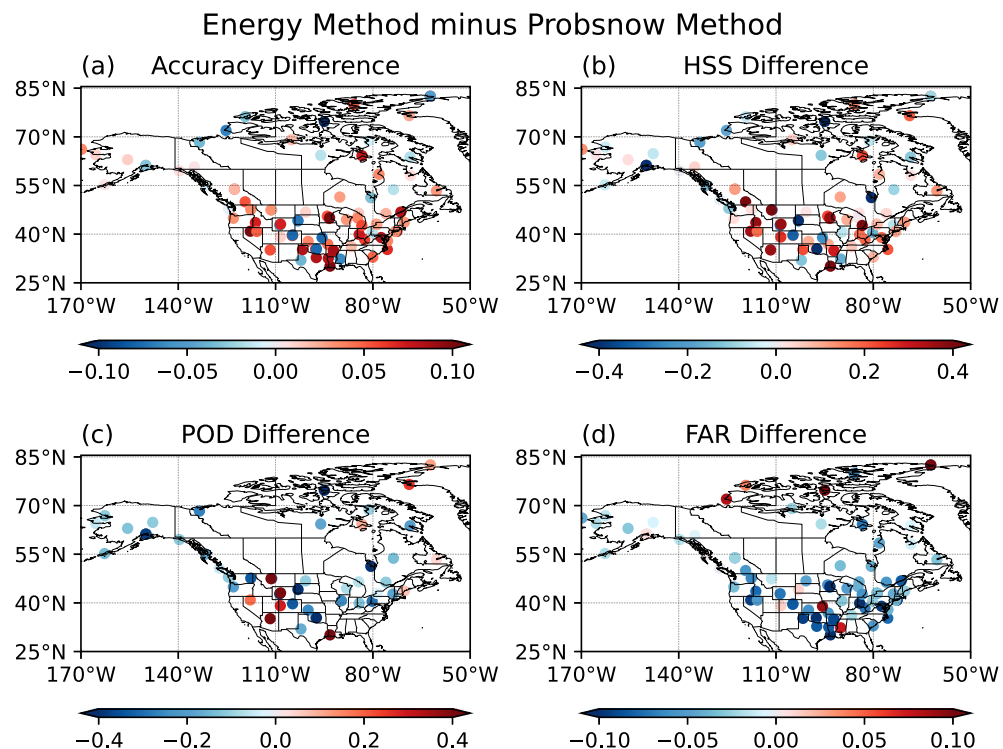


**Figure 11.** The difference of (a) accuracy, (b) Heidke skill score, (c) probability of detection, and (d) false alarm rate between the energy method and Probsnow method using a threshold of 50%.

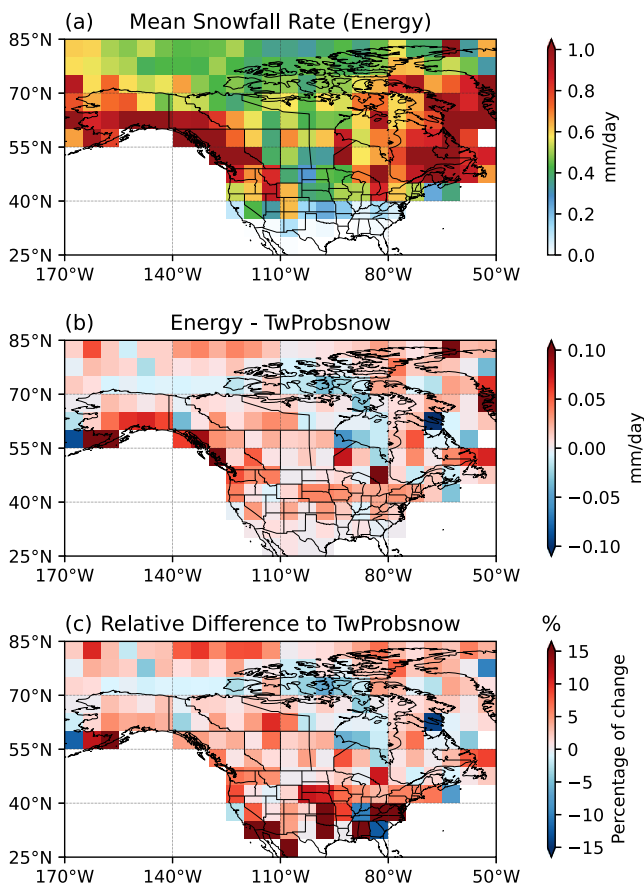


**Figure 12.** Application of the Energy method in satellite snowfall retrievals. (a) Annual mean snowfall rate for 2008, with the precipitation phase decided by the energy method with a threshold of 50%. (b) The difference in snowfall rates where phases are decided by the energy and the Probsnow methods (energy method minus Probsnow method) and (c) the relative difference compared to Probsnow method.

include the coastal Northeastern Pacific area, the western United States, the Great Lakes region, and eastern Canada. This distribution aligns with findings previously reported by Sims and Liu (2015).

Examining the differences in snowfall rates, Figure 12b reveals positive differences with the Probsnow method in most grids. Additionally, the relative difference, as depicted in Figure 12c, is most pronounced in lower latitudes, where snowfall rates are comparatively smaller in contrast to the mid to high latitudes. Figure S8 in Supporting Information S1 highlights prevalence of Type 2 soundings in higher latitudes north of 70°N, the eastern United States, and eastern Canada. The increased snowfall estimates north of 70°N and west of 100°W is possibly due to our improved prediction of snow phase in Type 2 soundings, while the differences along the coast of Northeast Pacific are largely attributed to our classification for Type 0 and Type 1 soundings.

In summary, the application of the energy method for precipitation phase classification yields notable differences in the resulting snowfall map compared to the Probsnow method, particularly in regions with varying snowfall patterns and Type 2 soundings, though the percentage of Type 2 soundings is smaller in the reanalysis than in observations (Figure S8 in Supporting Information S1). While it is necessary to rely on auxiliary data for satellite precipitation estimates, we remind the readers that the reanalysis profiles are likely to be influenced by its precipitation and modeled processes, and the results need to be interpreted with caution.

## 6. Summary and Discussion

In this study, we introduced an innovative precipitation phase classification scheme, referred to as the energy method, which features the calculation of the atmospheric melting and RE based on ice-bulb temperature vertical profiles. Solid (snow) and liquid (rain) phases are considered. We defined three types of soundings: Type 0 for entire atmosphere under 2 km from the surface either all below or all above freezing, Type 1 for profiles with a melting layer near the surface, and Type 2 for profiles with a melting layer aloft and a freezing layer beneath near the surface. This energy method particularly benefits Type 2 cases compared to previous methods. Our results highlight three key points:

1. Incorporation of the physical processes: By integrating the energy, our method addresses the essential process that a falling hydrometeor undergoes before reaching the ground, therefore adding a robust physical foundation for the phase classification scheme. This is a significant advancement compared to previous methods.
2. Importance of Type 2 soundings: The energy method demonstrates significant improvements in the classification of Type 2 soundings.
3. Classification threshold considerations: We provide classification functions for multiple thresholds of snow conditional probability from 30% to 80% in intervals of 10% to satisfy diverse needs in different applications.

For Type 1 soundings, our analysis demonstrates that utilizing ice-bulb temperature profiles outperforms using temperature profiles. Further combining surface temperature with the ME adds a physical foundation to using the ME alone. The energy method achieves similar performance as the Sims and Liu (2015) Probsnow method for the 50% threshold since both methods address the same atmospheric condition. The Probsnow method, which relies on lapse rate and surface wet-bulb temperature, essentially mirrors the definition of ME. More pronounced improvements are seen for the 70% threshold for Type 1 soundings, with an increase in HSS by 0.11.

In the case of Type 2 soundings, the Probsnow method exhibits limited skill due to its inability to capture the characteristics of inversion layers. In contrast, our energy method, which considers melting and RE derived from ice-bulb temperature soundings (TiME and TiRE), effectively represents the physical processes hydrometeors undergo before reaching the surface. With the combination of surface Ti, TiME and TiRE, the energy method significantly enhances classification metrics compared to the Probsnow method for the 50% threshold. Although

the POD decreases slightly, the FAR also decreases dramatically, indicating a more balanced prediction between rain and snow events. These improvements persist for the 70% threshold.

Station-level analysis reveals that the energy method reduces the magnitude of snow fraction bias compared to the Probsnow method for the 50% threshold. Furthermore, improvements in the accuracy and HSS are observed in over two-thirds of the stations. These improvements are particularly prominent in stations south of 50°N with a higher prevalence of Type 2 soundings, underscoring the significance of accurately predicting snow phase for Type 2 soundings by our energy method.

We also evaluate the differences in satellite radar snowfall retrieval patterns between the energy method and the Probsnow method. Negative changes are noted in the Pacific Northeast coast, while positive changes were observed in the eastern United States, eastern Canada, and the Arctic Ocean west of 110°W.

The energy method is built on observational data in the North American region. Looking ahead, it can be adapted for other regions with suitable observational data, provided there are weather station observations closely aligned with atmospheric vertical profiles. To apply this method to radar retrievals, auxiliary data on the vertical temperature structure should be collocated for ME and RE calculations. It is worth noting that reanalysis data tends to capture less Type 2 structure compared to observational data.

We developed the scheme based on ice-bulb temperature which is closer to the temperature of ice surface. We also provided the separation function coefficients derived from results based on wet-bulb temperature (Figures S9–S15 in Supporting Information S1). The major conclusions remain the same either we use ice-bulb temperature or wet-bulb temperature: comparable performance with Probsnow for Type 1 soundings, and desired significant improvements for Type 2 soundings. The performance difference between adopting the Ti-based or Tw-based scheme is small although the difference between Ti and Tw becomes bigger when the air gets drier. While we recommend the adoption of the ice-bulb temperature-based scheme, the choice of which scheme to use ultimately rests with the users.

In conclusion, our study presents a significant advancement in precipitation phase classification, with applications ranging from weather forecasting to hydrological modeling and radar snowfall retrievals. Compared to previous studies (Birk et al., 2021; Bourguin, 2000), our study uses more than 10 times of the data volume for algorithm development, reducing biases induced by the collocation between surface stations and soundings, and by the relatively scarce vertical spatial resolution. As more in situ observations accumulate in the future, the phase classification method proposed in this study can be further improved by training the algorithm by a more complete, time and space-intense observational data set. Additionally, we look forward to more studies exploring the physics of melting and freezing processes that will contribute to the phase classification.

## Data Availability Statement

NCEP ADP from 1975 to Feb 2007 (ds464.0) and from 1999 to present (ds461.0) are available from the Research Data Archive at the National Center for Atmospheric Research (National Centers for Environmental Prediction/National Weather Service/NOAA/U.S. Department of Commerce, 1980, 2004). IGRA version 2 (Durre et al., 2016) is available through the National Centers for Environmental Information. ERA5 hourly data on pressure levels (Hersbach et al., 2023a) and on single level (Hersbach et al., 2023b) are available at the Copernicus Climate Data Store. CloudSat 2B-GEOPROF Version 5 (Marchand et al., 2008) is available via the CloudSat Data Processing Center. The phase classification scheme (version 1.0) and the Python codes associated with this manuscript are licensed under MIT and published on Zenodo (Shi, 2024). Matplotlib version 3.8.0 is used to plot the figures in the manuscript (Hunter, 2007; The Matplotlib Development Team, 2023).

## Acknowledgments

This research has been supported by NASA CCST Grant 80NSSC22K1711 and JAXA AMSR3 grant ER3AMF201.

## References

- Auer, A. H. (1974). The rain versus snow threshold temperatures. *Weatherwise*, 27(2), 67–67. <https://doi.org/10.1080/00431672.1974.9931684>
- Barnes, L. R., Schultz, D. M., Grunfest, E. C., Hayden, M. H., & Benight, C. C. (2009). Corrigendum: False alarm rate or false alarm ratio? *Weather and Forecasting*, 24(5), 1452–1454. <https://doi.org/10.1175/2009WAF2222300.1>
- Barnhart, T. B., Molotch, N. P., Livneh, B., Harpold, A. A., Knowles, J. F., & Schneider, D. (2016). Snowmelt rate dictates streamflow. *Geophysical Research Letters*, 43(15), 8006–8016. <https://doi.org/10.1002/2016GL069690>
- Behrangi, A., Yin, X., Rajagopal, S., Stompoulis, D., & Ye, H. (2018). On distinguishing snowfall from rainfall using near-surface atmospheric information: Comparative analysis, uncertainties and hydrologic importance. *Quarterly Journal of the Royal Meteorological Society*, 144(S1), 89–102. <https://doi.org/10.1002/qj.3240>

- Berghuijs, W. R., Woods, R. A., & Hrachowitz, M. (2014). A precipitation shift from snow towards rain leads to a decrease in streamflow. *Nature Climate Change*, 4(7), 583–586. <https://doi.org/10.1038/nclimate2246>
- Birk, K., Lenning, E., Donofrio, K., & Friedlein, M. T. (2021). A revised Bourguin precipitation-type algorithm. *Weather and Forecasting*, 36(2), 425–438. <https://doi.org/10.1175/WAF-D-20-0118.1>
- Bocchieri, J. R. (1980). The objective use of upper air soundings to specify precipitation type. *Monthly Weather Review*, 108(5), 596–603. [https://doi.org/10.1175/1520-0493\(1980\)108<0596:TOUOUA>2.0.CO;2](https://doi.org/10.1175/1520-0493(1980)108<0596:TOUOUA>2.0.CO;2)
- Booth, B. (1973). A simplified snow predictor. *The Meteorological Magazine*, 102(4), 332–340. <https://doi.org/10.13182/nse89-a23646>
- Bourguin, P. (2000). A method to determine precipitation types. *Weather and Forecasting*, 15(5), 583–592. [https://doi.org/10.1175/1520-0434\(2000\)015<0583:AMTPT>2.0.CO;2](https://doi.org/10.1175/1520-0434(2000)015<0583:AMTPT>2.0.CO;2)
- Catto, J. L., Jakob, C., Berry, G., & Nicholls, N. (2012). Relating global precipitation to atmospheric fronts. *Geophysical Research Letters*, 39(10), L10805. <https://doi.org/10.1029/2012GL051736>
- Clow, D. W. (2010). Changes in the timing of snowmelt and streamflow in Colorado: A response to recent warming. *Journal of Climate*, 23(9), 2293–2306. <https://doi.org/10.1175/2009JCLI2951.1>
- Dai, A. (2008). Temperature and pressure dependence of the rain-snow phase transition over land and ocean. *Geophysical Research Letters*, 35(12), L12802. <https://doi.org/10.1029/2008GL033295>
- Dettinger, M. D., Knowles, N., & Cayan, D. R. (2015). Trends in snowfall versus rainfall in the Western United States—Revisited. In *Fall Meeting* (Vol. 2015, p. GC23B-1134). American Geophysical Union.
- Ding, B., Yang, K., Qin, J., Wang, L., Chen, Y., & He, X. (2014). The dependence of precipitation types on surface elevation and meteorological conditions and its parameterization. *Journal of Hydrology*, 513, 154–163. <https://doi.org/10.1016/j.jhydrol.2014.03.038>
- Durre, I., Xungang, Y., Vose, R. S., Applequist, S., & Arnfield, J. (2016). Integrated global radiosonde archive (IGRA) Version 2 [Dataset]. NOAA National Centers for Environmental Information, 10, V5X63X0Q. <https://www.ncdc.noaa.gov/access/metadata/landing-page/bin/iso?id=gov.noaa.ncdc:C00975>
- Ellis, A. W., & Sauter, K. (2017). The significance of snow to surface water supply: An empirical case study from the southwestern United States. *Physical Geography*, 38(3), 211–230. <https://doi.org/10.1080/02723646.2017.1281014>
- Fassnacht, S. R., Cherry, M. L., Venable, N. B. H., & Saavedra, F. (2016). Snow and albedo climate change impacts across the United States Northern Great Plains. *The Cryosphere*, 10(1), 329–339. <https://doi.org/10.5194/tc-10-329-2016>
- Fassnacht, S. R., Venable, N. B. H., Khishigbayar, J., & Cherry, M. L. (2013). *The probability of precipitation as snow derived from daily air temperature for high elevation areas of Colorado, United States* (Vol. 360, pp. 65–70). IAHS-AISH Publication.
- Feiccarino, J., Graff, W., Lundberg, A., Sandström, N., & Gustafsson, D. (2015). Meteorological knowledge useful for the improvement of snow rain separation in surface based models. *Hydrology*, 2(4), 4–288. <https://doi.org/10.3390/hydrology204026>
- Feng, S., & Hu, Q. (2007). Changes in winter snowfall/precipitation ratio in the contiguous United States. *Journal of Geophysical Research*, 112(D15), D15109. <https://doi.org/10.1029/2007JD008397>
- Froidurot, S., Zin, I., Hingray, B., & Gautheron, A. (2014). Sensitivity of precipitation phase over the Swiss Alps to different meteorological variables. *Journal of Hydrometeorology*, 15(2), 685–696. <https://doi.org/10.1175/JHM-D-13-073.1>
- Han, W., Xiao, C., Dou, T., & Ding, M. (2018). Changes in the proportion of precipitation occurring as rain in northern Canada during spring–summer from 1979–2015. *Advances in Atmospheric Sciences*, 35(9), 1129–1136. <https://doi.org/10.1007/s00376-018-7226-3>
- Harpold, A. A., Kaplan, M. L., Klos, P. Z., Link, T., McNamara, J. P., Rajagopal, S., et al. (2017). Rain or snow: Hydrologic processes, observations, prediction, and research needs. *Hydrology and Earth System Sciences*, 21(1), 1–22. <https://doi.org/10.5194/hess-21-1-2017>
- Hersbach, H., Bell, B., Berrisford, P., Biavati, G., Horányi, A., Muñoz Sabater, J., et al. (2023a). ERA5 hourly data on pressure levels from 1940 to present [Dataset]. *Copernicus Climate Change Service (C3S) Climate Data Store (CDS)*. <https://doi.org/10.24381/cds.bd0915c6>
- Hersbach, H., Bell, B., Berrisford, P., Biavati, G., Horányi, A., Muñoz Sabater, J., et al. (2023b). ERA5 hourly data on single levels from 1940 to present [Dataset]. *Copernicus Climate Change Service (C3S) Climate Data Store (CDS)*. <https://doi.org/10.24381/cds.adbb2d47>
- Heymsfield, A. J., Bansemer, A., Theis, A., & Schmitt, C. (2021). Survival of snow in the melting layer: Relative humidity influence. *Journal of the Atmospheric Sciences*, 78(6), 1823–1845. <https://doi.org/10.1175/JAS-D-20-0353.1>
- Huffman, G. J., Bolvin, D. T., Braithwaite, D., Hsu, K.-L., Joyce, R. J., Kidd, C., et al. (2020). Integrated multi-satellite retrievals for the global precipitation measurement (GPM) mission (IMERG). In V. Levizzani, C. Kidd, D. B. Kirschbaum, C. D. Kummerow, K. Nakamura, & F. J. Turk (Eds.), *Advances in Global Change Research* (Vol. 67, pp. 343–353). Springer Nature. [https://doi.org/10.1007/978-3-030-24568-9\\_19](https://doi.org/10.1007/978-3-030-24568-9_19)
- Hunter, J. D. (2007). Matplotlib: A 2D graphics environment [Software]. *Computing in Science & Engineering*, 9(3), 90–95. <https://doi.org/10.1109/MCSE.2007.55>
- Irannezhad, M., Ronkanen, A.-K., Kiani, S., Chen, D., & Kløve, B. (2017). Long-term variability and trends in annual snowfall/total precipitation ratio in Finland and the role of atmospheric circulation patterns. *Cold Regions Science and Technology*, 143, 23–31. <https://doi.org/10.1016/j.coldregions.2017.08.008>
- Iribarne, J. V., & Godson, W. L. (1973). Area computation and energy integrals. In B. M. McCormac (Ed.), *Atmospheric thermodynamics* (Vol. 6, pp. 91–96). D. Reidel Publishing Company.
- Jennings, K. S., Winchell, T. S., Livneh, B., & Molotch, N. P. (2018). Spatial variation of the rain–snow temperature threshold across the Northern Hemisphere. *Nature Communications*, 9(1), 1148. <https://doi.org/10.1038/s41467-018-03629-7>
- Knowles, N., Dettinger, M. D., & Cayan, D. R. (2006). Trends in snowfall versus rainfall in the western United States. *Journal of Climate*, 19(18), 4545–4559. <https://doi.org/10.1175/JCLI3850.1>
- Kubota, T., Aonashi, K., Ushio, T., Shige, S., Takayabu, Y. N., Kachi, M., et al. (2020). Global Satellite Mapping of Precipitation (GSMaP) products in the GPM era. In V. Levizzani, C. Kidd, D. B. Kirschbaum, C. D. Kummerow, K. Nakamura, & F. J. Turk (Eds.), *Advances in Global Change Research* (Vol. 67, pp. 355–371). Springer Nature. [https://doi.org/10.1007/978-3-030-24568-9\\_20](https://doi.org/10.1007/978-3-030-24568-9_20)
- Liu, G. (2008). Deriving snow cloud characteristics from CloudSat observations. *Journal of Geophysical Research*, 113(D8), D00A09. <https://doi.org/10.1029/2007JD009766>
- Lumb, F. (1961). The problem of forecasting the downward penetration of snow. *The Meteorological Magazine*, 90, 310–319.
- Lumb, F. (1963). Downward penetration of snow in relation to the intensity of precipitation. *The Meteorological Magazine*, 92, 1–14.
- Maahn, M., Burgard, C., Crewell, S., Gorodetskaya, I. V., Kneifel, S., Lhermitte, S., et al. (2014). How does the spaceborne radar blind zone affect derived surface snowfall statistics in polar regions? *Journal of Geophysical Research: Atmospheres*, 119(24), 13604–13620. <https://doi.org/10.1002/2014JD022079>
- Marchand, R., Mace, G. G., Ackerman, T., & Stephens, G. (2008). Hydrometeor detection using Cloudsat—An Earth-orbiting 94-GHz cloud radar [Dataset]. *Journal of Atmospheric and Oceanic Technology*, 25(4), 519–533. <https://doi.org/10.1175/2007JTECHA1006.1>

- Marks, D., Winstral, A., Reba, M., Pomeroy, J., & Kumar, M. (2013). An evaluation of methods for determining during-storm precipitation phase and the rain/snow transition elevation at the surface in a mountain basin. *Advances in Water Resources*, 55, 98–110. <https://doi.org/10.1016/j.advwatres.2012.11.012>
- Murray, R. (1952). Rain and snow in relation to the 1000-700-mb. And 1000-500-mb thicknesses and the freezing level. *The Meteorological Magazine*, 81, 955.
- National Centers for Environmental Prediction/National Weather Service/NOAA/U.S. Department of Commerce. (1980). NCEP ADP operational global surface observations, February 1975–February 2007 [Dataset]. *Research Data Archive at the National Center for Atmospheric Research, Computational and Information Systems Laboratory*. <https://doi.org/10.5065/E6NW-HY91>
- National Centers for Environmental Prediction, National Weather Service, NOAA, U.S. Department of Commerce. (2004). NCEP ADP global surface observational weather data, October 1999—Continuing [Dataset]. *Research Data Archive at the National Center for Atmospheric Research, Computational and Information Systems Laboratory*. <https://doi.org/10.5065/4F4P-E398>
- Pandolfo, J. P. (1957). An objective method for forecasting precipitation type during the winter months at New York City. *Bulletin of the American Meteorological Society*, 38(10), 571–574. <https://doi.org/10.1175/1520-0477-38.10.571>
- Penn, S. (1957). The prediction of snow vs. rain. In *Forecasting Guide* (Vol. 2, p. 29). US Department of Commerce, Weather Bureau.
- Pettersen, C., Bliven, L. F., Kulie, M. S., Wood, N. B., Shates, J. A., Anderson, J., et al. (2021). The precipitation imaging package: Phase partitioning capabilities. *Remote Sensing*, 13(11), 11. <https://doi.org/10.3390/rs13112183>
- Randel, D. L., Kummerow, C. D., & Ringerud, S. (2020). The Goddard Profiling (GPROF) precipitation retrieval algorithm. In V. Levizzani, C. Kidd, D. B. Kirschbaum, C. D. Kummerow, K. Nakamura, & F. J. Turk (Eds.), *Satellite precipitation measurement, Advances in Global Change Research* (Vol. 67, pp. 141–152). Springer Nature. [https://doi.org/10.1007/978-3-030-24568-9\\_8](https://doi.org/10.1007/978-3-030-24568-9_8)
- Serquet, G., Marty, C., Dulex, J.-P., & Rebetez, M. (2011). Seasonal trends and temperature dependence of the snowfall/precipitation-day ratio in Switzerland. *Geophysical Research Letters*, 38(7), L07703. <https://doi.org/10.1029/2011GL046976>
- Shi, S. (2024). EnergyPhaseClassification: Version 1.0 [Software]. Zenodo. <https://doi.org/10.5281/zenodo.10845973>
- Shi, S., & Liu, G. (2021). The latitudinal dependence in the trend of snow event to precipitation event ratio. *Scientific Reports*, 11(1), 18112. <https://doi.org/10.1038/s41598-021-97451-9>
- Sims, E. M., & Liu, G. (2015). A parameterization of the probability of snow–rain transition. *Journal of Hydrometeorology*, 16(4), 1466–1477. <https://doi.org/10.1175/JHM-D-14-0211.1>
- Tharwat, A., Gaber, T., Ibrahim, A., & Hassanien, A. E. (2017). Linear discriminant analysis: A detailed tutorial. *AI Communications*, 30(2), 169–190. <https://doi.org/10.3233/AIC-170729>
- The Matplotlib Development Team. (2023). Matplotlib: Visualization with Python (v3.8.0) [Software]. Zenodo. <https://doi.org/10.5281/zenodo.8347255>
- Thériault, J. M., Stewart, R. E., Milbrandt, J. A., & Yau, M. K. (2006). On the simulation of winter precipitation types. *Journal of Geophysical Research*, 111(D18), D18202. <https://doi.org/10.1029/2005JD006665>
- Wang, J., Zhang, M., Wang, S., Ren, Z., Che, Y., Qiang, F., & Qu, D. (2016). Decrease in snowfall/rainfall ratio in the Tibetan Plateau from 1961 to 2013. *Journal of Geographical Sciences*, 26(9), 1277–1288. <https://doi.org/10.1007/s11442-016-1326-8>
- Wang, Y.-H., Broxton, P., Fang, Y., Behrangi, A., Barlage, M., Zeng, X., & Niu, G.-Y. (2019). A wet-bulb temperature-based rain-snow partitioning scheme improves snowpack prediction over the drier western United States. *Geophysical Research Letters*, 46(23), 13825–13835. <https://doi.org/10.1029/2019GL085722>
- Ye, H., Cohen, J., & Rawlins, M. (2013). Discrimination of solid from liquid precipitation over Northern Eurasia using surface atmospheric conditions. *Journal of Hydrometeorology*, 14(4), 1345–1355. <https://doi.org/10.1175/JHM-D-12-0164.1>